

Article

Design and Characterization of Ag@Cu₂O-rGO Nanocomposite for the *p*-Nitrophenol Reduction

Chao Song ^{1,2,*}, Shuang Guo ² and Lei Chen ^{2,*} ¹ Teaching Affairs Office, Jilin Normal University, Siping 136000, China² College of Chemistry, Jilin Normal University, Siping 136000, China; guoshuang0420@163.com

* Correspondence: songchao@jlnu.edu.cn (C.S.); chenlei@jlnu.edu.cn (L.C.); Tel.: +86-434-329-2350 (C.S.)

Abstract: In this paper, we designed Ag nanoparticles coated with a Cu₂O shell, which was successfully decorated on reduced graphene oxide (rGO) via a solid-state self-reduction. The Cu₂O, Ag@Cu₂O, and Ag@Cu₂O-rGO nanocomposites were synthesized and characterized using scanning electron microscopy (SEM), transmission electron microscopy (TEM), UV-Vis, and XPS to evaluate the properties of the composites. In order to compare the chemical catalytic activity, the Cu₂O, Ag@Cu₂O, and Ag@Cu₂O-rGO nanocomposites were employed for the catalytic reduction of *p*-nitrophenol (4-NP) into *p*-aminophenol (4-AP) in aqueous solution. The Ag@Cu₂O-rGO nanocomposite exhibited excellent catalytic activity due to the intense interaction and high degree of electron transfer among Ag, Cu₂O, and rGO. The rGO acted as the platform to bridge the isolated nanoparticles; furthermore, the electrons could quickly transfer from the Ag core to the Cu₂O shell, which improved the chemical catalytic efficiency.

Keywords: Ag@Cu₂O-rGO; chemical catalytic; *p*-nitrophenol



Citation: Song, C.; Guo, S.; Chen, L. Design and Characterization of Ag@Cu₂O-rGO Nanocomposite for the *p*-Nitrophenol Reduction. *Catalysts* **2021**, *11*, 43. <https://doi.org/10.3390/catal11010043>

Received: 20 November 2020

Accepted: 29 December 2020

Published: 31 December 2020

Publisher's Note: MDPI stays neutral with regard to jurisdictional claims in published maps and institutional affiliations.



Copyright: © 2020 by the authors. Licensee MDPI, Basel, Switzerland. This article is an open access article distributed under the terms and conditions of the Creative Commons Attribution (CC BY) license (<https://creativecommons.org/licenses/by/4.0/>).

1. Introduction

Two-dimensional (2D) materials are a new kind of materials, whose transverse size is more than 100 nm, or even several microns or larger, but the thickness is only on the single or several atomic scale, has a large specific surface area, and can provide a large number of reaction sites [1–4]. In addition, 2D materials have unique physical and chemical properties due to their unique electronic plane motion space. Excellent structural properties, and unique physical and chemical properties give 2D materials a wide range of potential applications, such as catalysis, electronics and optoelectronics, energy storage and conversion, detector and sensor functions, and biomedicine [5–10]. The rapid development of 2D materials has enriched the types of catalysts to effectively overcome the limitations of a single type of catalyst, and has made outstanding contributions to the improvement of catalytic efficiency. Two-dimensional catalytic materials have many interesting characteristics, such as porous structure, high specific surface area, good crystallinity, rich host-guest selectivity, better charge carrier separation, and rich surface-active sites, which are excellent candidates for the synthesis of catalytic materials [11–15].

Graphene has all the properties of ultrathin 2D nanomaterials, such as physical, electronic, chemical, and optical properties, so it has a wide range of applications. Due to the mechanical and electronic properties of monolayers or several layers of 2D graphene, it has become the focus of nano electronic research. Its ultra-thin property makes it resistant to short channel effects, and it has high flexibility. Accordingly, graphene materials have been widely used as catalysts in photocatalysis, electrocatalysis, and chemocatalysis systems. In addition, its excellent performance also makes it a hot material in the fields of batteries, super-capacitors, solar cells, detection, and sensing [16–19].

Two-dimensional nano engineering plays an important role in the rational design of catalysts owing to its controllable composition, structure, and interface characteristics. The catalytic materials based on 2D materials are expected to show more meaningful functions.

It is expected that 2D based catalysts with high specific surface area and good selectivity for host and guest separation can be provided. However, 2D materials have some limitations in the field of catalysis systems. Some 2D materials have poor stability. For example, black scales are very easy to oxidize and decompose or absorb water to form phosphoric acid in natural environments; the intrinsic band gap energy of g-C₃N₄ is small, and the carrier energy excited by light is not enough to catalyze the degradation of pollutant molecules [20]. The synthesis process of some 2D materials, such as organic skeleton, black phosphorus, and inorganic hybrid perovskite, is complex and cannot be produced in a large quantity, which limits its wide application in the field of catalysis [21–23].

Metal and metal oxide composites are considered to be the unique carriers of promising functional materials [24,25]. Metal and metal oxide nanoparticles are much more stable than single components. The surface area of photocatalyst is expanded by adjusting its morphology and composition. In the composite structure, the separation of electron–hole pairs can be promoted by carrier transport and electron coupling. Metal semiconductor core–shell nanomaterials exhibit excellent catalytic properties. Metal materials as the core or surface-modified metal oxides is a common and feasible conventional material for catalyst support. Compared with metals or semiconductors, metal semiconductor composites have many different properties that are easy to control, such as phonon coupling strength, plasma induced catalysis, and plasma induced resonance energy transfer [26,27]. When the charge transfer occurs between metal–metal and metal–semiconductor, the physical and chemical properties of materials change noticeably. This provides an ideal platform to study multi-functional nanomaterials.

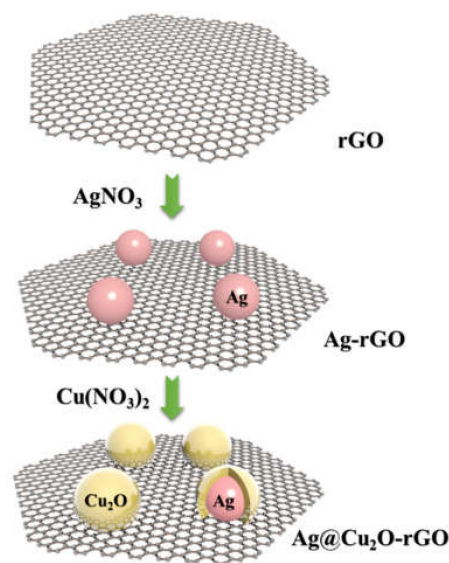
In order to solve the single mechanism and the limitations of material properties in the field of materials science, a unique ternary platform/core–shell nanostructure was prepared using the wet chemical method. Ag–Cu₂O composite has unique properties compared with pure Cu₂O, and the formation of the heterojunction between Ag and Cu₂O exhibited promising photoelectric and catalytic performances. The metallic Ag can provide a large number of free electrons, and the large energy level difference between Ag nanoparticles and Cu₂O promotes the transfer of photogenerated electrons between the Cu₂O shell and the Ag core. By introducing the reduced graphene oxide (rGO), the researchers found that ternary composites of Ag, Cu₂O, and rGO exhibited an excellent catalytic property. Xu et al. fabricated the Ag@Cu₂O–rGO composite through a simple one-pot, two-stage reduction of the synthetic route at room temperature without any surfactants [28]. The direct junction and interaction between Ag and Cu₂O are beneficial for charge transfer in the ternary composites of Ag, Cu₂O, and rGO. Guo et al. reported a two-step in situ reduction procedure for preparing ternary Ag@Cu₂O–rGO nanocomposites in order to overcome the instability of Ag nanoparticles [29]. Ag@Cu₂O–rGO nanocomposites exhibited excellent peroxidase-like activity, which was based on surface modification of Ag nanoparticles by Cu₂O spheres, and attached to the surface of rGO. Therefore, rGO, an excellent electron transport material, combined with Ag@Cu₂O shows excellent catalytic and carrier transport properties. The multi-interface coupling and multi porous structure of Ag@Cu₂O–rGO nanostructures exhibited excellent performance in the chemocatalysis of *p*-nitrophenol (4-NP), which proved the special properties of this composite structure.

2. Results and Discussion

The synthesis of Ag@Cu₂O core–shell and Ag@Cu₂O–rGO composite structure used a simple wet chemical method. The fabrication process is shown in Scheme 1.

First, the rGO was prepared by using Hummer and Offeman's two-part oxidation method [29]. Second, the Ag NPs were decorated on the rGO based on the modified Lee and Meisel sol preparation method [28]. The morphology and internal structures of samples were analyzed by scanning electron microscopy (SEM) and transmission electron microscopy (TEM) images, as shown in Figure 1. The spherical Cu₂O nanoparticles were about 200 nm, and the surface was rough and porous (Figure 1D). The TEM of Ag@Cu₂O composites is shown in Figure 1F. Ag NPs (50–70 nm) were coated with the Cu₂O shell,

the surface of which was rough and porous. A rough and porous structure is good for the target adsorption. In order to obtain the Ag@Cu₂O-rGO composites, the Cu₂O was coated on the surface of the Ag NPs based on a simple wet chemical method and was decorated on the rGO. The Ag@Cu₂O-rGO composite structure still maintained a 2D structure of rGO after a series of surface modification, and its surface was arranged with neat spherical nanoparticles, as shown in Figure 1C. Further research showed that the nanoparticles on the rGO surface comprised the core-shell structure, which was proved by the TEM image, as shown in Figure 1F. Pure Cu₂O and Ag@Cu₂O structures were also studied for comparative analysis, as shown in Figure 1A,B,D,E. The SEM and TEM images of the Ag@Cu₂O and Ag@Cu₂O-rGO showed that the two structures had similar core-shell structures, except for the rGO of the substrate. More importantly, the surface of Cu₂O had a rough porous structure, and more active sites were exposed to interact with the targets.



Scheme 1. The schematic of the preparation of the Ag@Cu₂O-rGO composites.

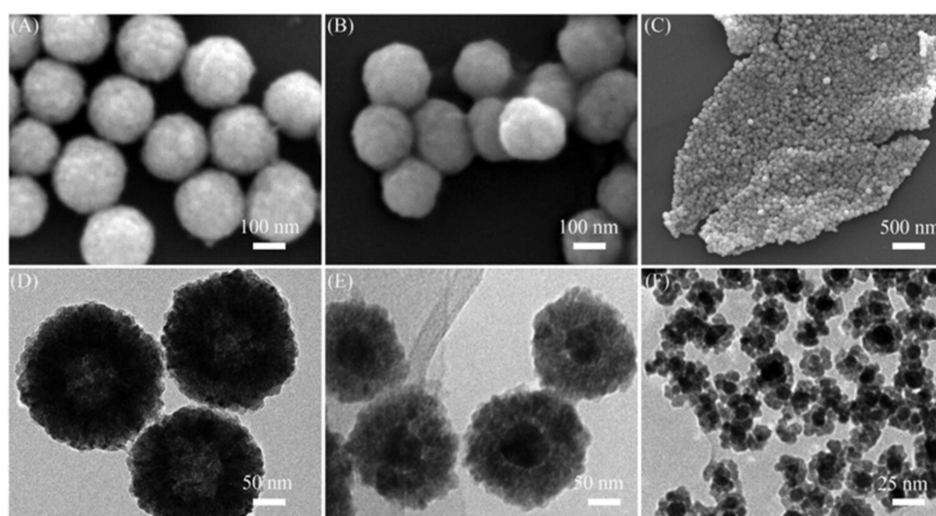


Figure 1. The scanning electron microscopy (SEM) and transmission electron microscopy (TEM) images of Cu₂O (A and D), Ag@Cu₂O (B and E), and Ag@Cu₂O-rGO (C and F) composites.

The composites were studied by XPS spectra in order to confirm the material composition, as shown in Figure 2A. The Cu 2p (Figure 2B) and the Ag 3d (Figure 2C) peaks

could be clearly seen from the XPS spectra of Ag@Cu₂O and Ag@Cu₂O-rGO structures, which indicated the successful synthesis of this structure. As shown in Figure 2B, we found that the binding energy of Cu 2p_{3/2} and Cu 2p_{1/2} located at 932.0 and 951.9 eV of the Ag@Cu₂O and Ag@Cu₂O-rGO, respectively, were consistent with the binding energy of the Cu₂O, which indicated the formation of Cu₂O particles. In Figure 2C, the peaks of Ag 3d at 367.7 and 373.8 eV assigned to the Ag 3d_{5/2} and Ag 3d_{3/2}, respectively, demonstrated the formation of pure metallic Ag [29]. Moreover, we found that the Ag 3d_{3/2} peak in Ag@Cu₂O-rGO had a slight shift to higher binding energy compared with the Ag 3d_{3/2} peak in Ag@Cu₂O, which was due to the transfer of free electrons on the Ag surface.

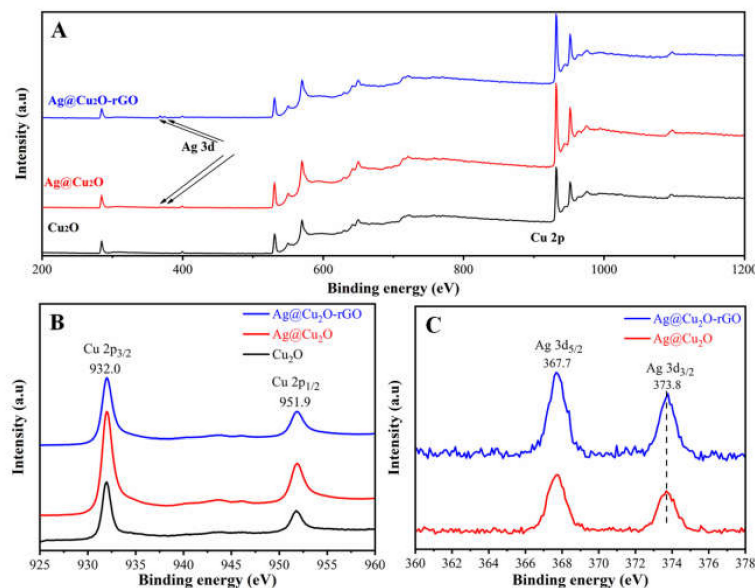


Figure 2. (A) The survey XPS, (B) Cu 2p, and (C) Ag 3d spectra of Cu₂O, Ag@Cu₂O, and Ag@Cu₂O-rGO composite structures.

In order to study the optical response of different materials, the UV–Vis absorbance spectra of Cu₂O, Ag@Cu₂O, and Ag@Cu₂O-rGO composite structures were measured in order to study the optical response of different materials, as shown in Figure 3. Compared with pure Cu₂O nanoparticles, the Ag@Cu₂O core–shell structure had a plasma absorption band at about 500–700 nm. This was assigned to the geometry-dependent light absorption and scattering from the Ag@Cu₂O composite. In addition, the inherent absorption band of Cu₂O also appeared as a significant blue shift due to the different Fermi levels of the Ag core and Cu₂O shell. Moreover, the variation of the Cu₂O cluster size also caused the blue shift of the Cu₂O absorption band. When the rGO was added to the composite structure, the plasma peak assigned to the Ag@Cu₂O core–shell structure was enhanced, which was possible because of the interface coupling between Cu₂O and rGO that induced the photo-response of the Cu₂O increase around 600 nm.

Organic dyes, pesticides, and persistent organic pollutants are harmful to humans and are currently a global environmental problem that is of great concern. They can seriously pollute the soil and endanger human safety. The development of a method for their catalytic degradation is very important. The molecule 4-NP is an intermediate in the synthesis of pesticides, drugs, and dyes. Since 4-NP is a common pollutant and is potentially harmful, researchers have developed a variety of catalytic materials to degrade it. To evaluate the catalytic activity of the Cu₂O, Ag@Cu₂O, and Ag@Cu₂O-rGO composite structures, we employed 4-NP as the probe molecule. The synthesized Cu₂O, Ag@Cu₂O, and Ag@Cu₂O-rGO were utilized to catalyze the 4-NP (10^{−3} M) solution in the presence sodium borohydride (NaBH₄). The absorption peak of 4-NP was around 340 nm (Figure 4). After NaBH₄ was added, 4-NP became ionic, and the absorption peak was around 400 nm (Figure 4). In a cu-

vette, 2 mL of deionized water and 0.1 mL (0.005 mol/L) of 4-NP were added. Then, a freshly prepared NaBH_4 (0.2 mol/L) solution was added to the transparent solution. The color of the solution changed to bright yellow. Subsequently, 5 μL of Cu_2O , $\text{Ag@Cu}_2\text{O}$, and $\text{Ag@Cu}_2\text{O-rGO}$ solutions were added separately to perform catalytic reductions (Figure 4A,B). It took 48 min and 36 min, respectively, to catalyze 4-NP completely by using Cu_2O and $\text{Ag@Cu}_2\text{O}$ as the catalysts (Figure 5A,B). Owing to the combination of Ag and Cu_2O , the work function of Ag was smaller than that of Cu_2O , which made the electrons transfer to Ag. There are numerous positive charges on the surface of Cu_2O , which attracts 4-NP to the area near $\text{Ag@Cu}_2\text{O}$ to accelerate the degradation of BH_4^- catalysis. Moreover, rGO acted as the electron transfer platform, causing a high catalyst efficiency.

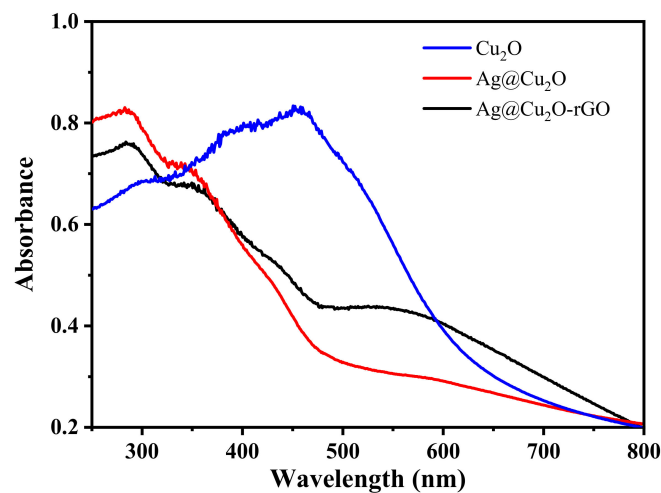


Figure 3. UV-Vis absorbance spectra of Cu_2O , $\text{Ag@Cu}_2\text{O}$, and $\text{Ag@Cu}_2\text{O-rGO}$ composite structures.

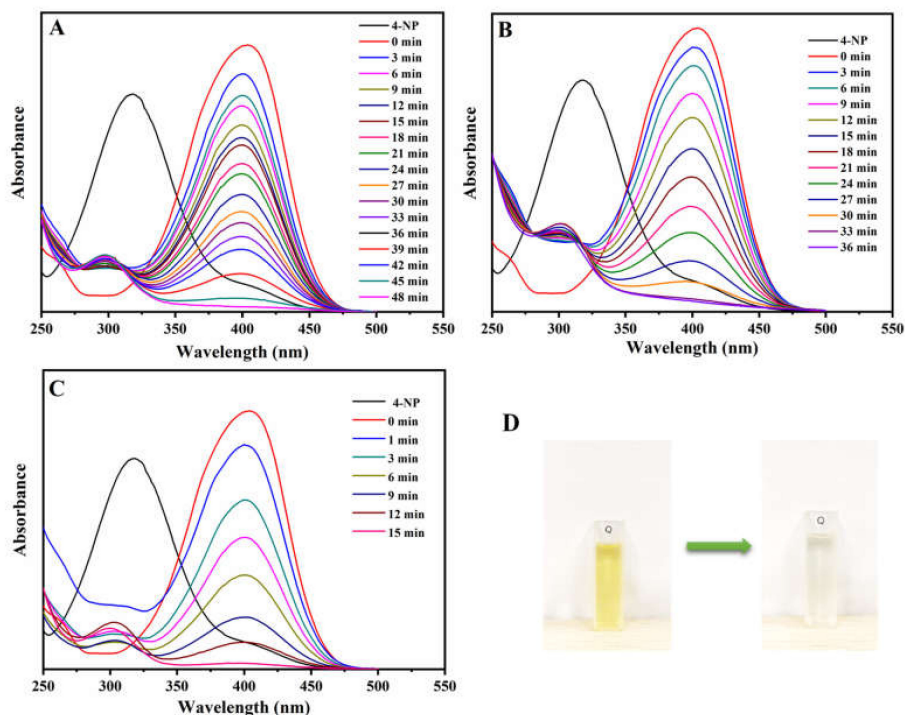


Figure 4. UV-Vis absorption spectra of the reduction of 4-NP by NaBH_4 in the presence of (A) Cu_2O ($t = 48$ min), (B) $\text{Ag@Cu}_2\text{O}$ ($t = 36$ min), and (C) $\text{Ag@Cu}_2\text{O-rGO}$ ($t = 15$ min). (D) Photographs of the catalytic reduction of 4-NP by NaBH_4 in the absence and presence of $\text{Ag@Cu}_2\text{O-rGO}$ ($t = 15$ min).

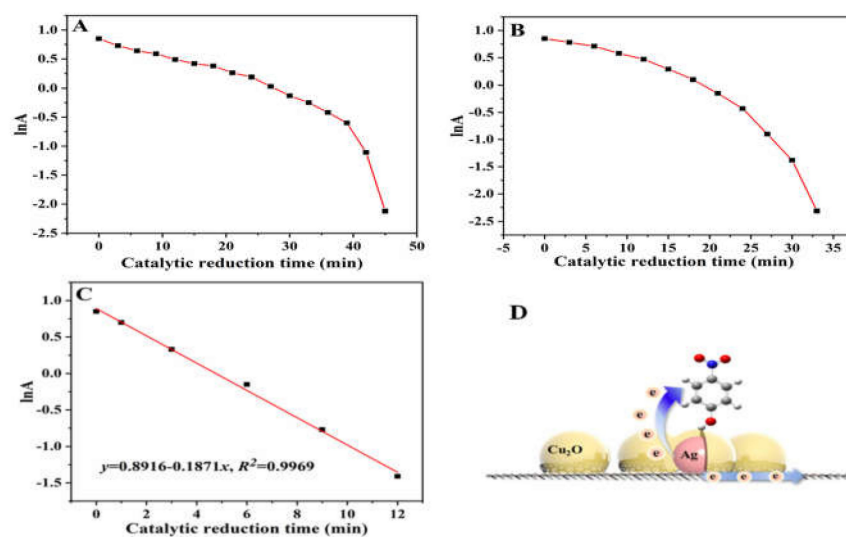


Figure 5. The logarithm of the absorbance at 400 nm vs. catalytic reduction time by using (A) Cu₂O, (B) Ag@Cu₂O, and (C) Ag@Cu₂O-rGO materials. (D) The schematic of the catalytic mechanism of 4-NP on the Ag@Cu₂O-rGO interface. The 4-NP is adsorbed on Ag@Cu₂O-rGO, BH₄⁻ ion provides electrons for catalysis, and the electrons migrate between Ag@Cu₂O and rGO in a depletion region near the Ag@Cu₂O-rGO interface, forming an electron-rich region. These excess electrons in the presence of rGO promote the absorption of electrons by 4-NP molecules near these regions. Thus, the catalytic efficiency is considerably improved.

The strong adsorption capacity of Ag@Cu₂O-rGO encouraged us to use this material to reduce 4-NP for water restoration [30]. The degradation of 4-NP in the presence of NaBH₄ using Ag@Cu₂O-rGO was completed. This classic reaction degrades 4-NP in the presence of NaBH₄ through nanocatalysis, because the reaction is fast and easy to characterize and is often reported. The process of reducing 4-NP to 4-aminophenol (4-AP) using Ag@Cu₂O-rGO was observed by UV-Vis absorption spectroscopy (Figure 4C). The Ag@Cu₂O-rGO synthetic material is porous and can provide a large number of active sites. This characteristic plays a very good role in catalysis. In the catalytic reaction, electrons on the Ag@Cu₂O surface are transported to BH₄⁻, so 4-NP is reduced by BH₄⁻ to 4-AP. It took 15 min to catalyze 4-NP completely by using the Ag@Cu₂O-rGO nanocomposite. Compared with Ag@Cu₂O, the catalytic efficiency of Ag@Cu₂O-rGO nanoparticles was quite high. Here, when 4-NP was adsorbed on the catalyst, the BH₄⁻ ion provided electrons for catalysis. Therefore, electrons migrated between the Ag@Cu₂O and rGO in a depletion region near the Ag@Cu₂O-rGO interface, forming an electron-rich region. These excess electrons in the presence of rGO promoted the absorption of electrons by 4-NP molecules near these regions (Figure 5D). Thus, the catalytic efficiency was considerably improved by introducing the rGO. If there are more interfaces, there will be more areas with residual electrons [31]. Therefore, when introducing the rGO as the platform for Ag@Cu₂O, the catalytic activity increases dramatically. The linear relationship between absorption logarithm (ln(A)) and time (t) showed that the reduction of 4-NP with Ag@Cu₂O-rGO conformed to pseudo first-order kinetics. As seen in Figure 5C, the 4-NP reduction rate was 0.19 min⁻¹.

The UV absorption spectra of the reduction reaction are shown in Figure 4A–C, and the images before (yellow) and after (colorless) the reaction are shown in Figure 4D. The high adsorption capacity of Ag@Cu₂O-rGO nanoparticles was due to their abundant active sites and could be used as a catalyst. This also clearly showed that Ag@Cu₂O-rGO nanoparticles showed excellent catalytic efficiency and trace catalytic ability. Ag@Cu₂O-rGO in particular had a significant catalytic efficiency compared to Ag@Cu₂O and Cu₂O (Figure 5). Two-dimensional rGO had very good electron transport ability. Therefore, rGO, as a charge transfer platform, can transfer electrons from Ag nanoparticles to the Cu₂O shell or adjacent core-shell structure, so as to improve electronic utilization efficiency.

3. Materials and Methods

3.1. Materials

The synthesis of graphene oxide (GO) is mainly based on graphite powder, potassium persulfate ($K_2S_2O_8$, AR), phosphorus pentoxide (P_2O_5 , AR), potassium permanganate ($KMnO_4$), hydrogen peroxide (H_2O_2 , 30 wt.%), sulfuric acid (H_2SO_4 , 98.98 wt.%), and phosphoric acid (H_3PO_4 , 85 wt.%) reagents. The main materials for GO modification include anhydrous ethanol (C_2H_6O , ≥ 99.8 wt.%), sodium citrate dihydrate ($C_6H_5Na_3O_7 \cdot 2H_2O$, AR), silver nitrate ($AgNO_3$, AR), hydrazine hydrate ($H_4N_2 \cdot H_2O$, 85 wt.%), polyvinylpyrrolidone ($(C_6H_9NO)_n$, PVP K30, AR), and copper(II) nitrate trihydrate ($Cu(NO_3)_2 \cdot 3H_2O$, AR). All chemicals in this experiment were purchased from Sinopharm Chemical Reagent Co., Ltd (Shanghai, China) and used as received without further treatment. The preparative solution in this study was deionized water.

3.2. Synthesis of Composite Materials

3.2.1. Synthesis of Ag@Cu₂O Core–Shell Structure

First, uniform-sized Ag nanoparticles (Ag NPs) are prepared based on the slightly improved Lee and Meisel sol preparation method [32]; the detailed operation is as follows: (1) 36 mg $AgNO_3$ was added to a three-necked flask, and then 200 mL of deionized water was added to the flask, condensed, and refluxed at 90 °C and stirred magnetically until it boiled slightly. (2) After adjusting the heating temperature to 85 °C, 4 mL of a uniformly dissolved sodium citrate aqueous solution (1 wt.%) was quickly added into the three-necked flask, and the solution gradually turned yellow–green after 40 min. Thus, Ag NPs with uniform size were obtained. Then, the Ag@Cu₂O core–shell structure was synthesized, in which a layer of Cu₂O shell was grown on the surface of Ag NPs based on a simple wet chemical method. The detailed operation is as follows: (1) 1 g of PVP was dissolved uniformly in 50 mL of $Cu(NO_3)_2$ aqueous solution (0.01 M); (2) 20 mL of the previously prepared Ag sol solution was added to $Cu(NO_3)_2$ solution; (3) the above solution was magnetically stirred at 300 rpm at room temperature, and then $H_4N_2 \cdot H_2O$ (68 μ L, 35 wt.%) was added to the solution and kept it for 90 s. The obtained solution was centrifuged and cleaned twice to obtain Ag@Cu₂O core–shell nanoparticles with a uniform structure.

3.2.2. Synthesis of Ag@Cu₂O-rGO Composite Structure

Firstly, the GO with a large number of functional groups on the surface was prepared by the modified Hummer and Offeman's two-part oxidation method [33]. Secondly, uniform modification of the surface of GO was performed by Ag NPs based on a modified Lee and Meisel method, in which 1 mg GO was added during the synthesis of Ag NPs to form the Ag-rGO structure. Finally, the synthesis of the Ag-rGO composite structure was obtained. In order to coat Cu₂O on the Ag nanoparticles, which were decorated on the rGO, the detailed operation is as follows: (1) 1 g of PVP was dissolved uniformly in 50 mL of $Cu(NO_3)_2$ aqueous solution (0.01 M); (2) 20 mL of the previously prepared Ag-rGO composite solution was added to $Cu(NO_3)_2$ solution; (3) the above solution was magnetically stirred at 300 rpm at room temperature, and then $H_4N_2 \cdot H_2O$ (68 μ L, 35 wt.%) was added to the solution and stirred for 90 s. The obtained solution was centrifuged and cleaned twice to obtain the Ag@Cu₂O-rGO composite.

3.3. Catalytic Degradation Experiment

In each cuvette, Cu₂O, Ag@Cu₂O, and Ag@Cu₂O-rGO nanoparticles were mixed with 0.1 mL of 0.005 mol/L 4-NP, after which the fresh $NaBH_4$ (0.2 mol/L) solution was added. The solution changed from colorless to bright yellow. With increasing catalytic time, the bright yellow solution changed to colorless.

3.4. Characterization

The surface morphology of the composite structure was studied by a JEOL 7800F scanning electron microscopy (SEM) under 5.0 kV accelerating voltage. Internal structures

of the composite structure were investigated by a Hitachi H-800 transmission electron microscopy (TEM) under 200 kV accelerating voltage. The elemental compositions of the composite structure were studied by X-ray photoelectron spectroscopy (XPS) with a Thermo Scientific ESCALAB 250Xi A1440 system. UV–Vis absorption properties of the composite structure were studied using a Shimadzu 3600 spectrometer. The concentrations of the signal molecules were obtained by a Hitachi U-4100 spectrophotometer based on the absorption characteristics of the signal molecules.

4. Conclusions

In summary, the colloidal chemistry method was employed to synthesize Ag@Cu₂O-rGO, which exhibited an excellent chemical catalyst property for 4-NP. Compared with Cu₂O and Ag@Cu₂O, Ag@Cu₂O-rGO showed the best catalytic performance, which was due to the excellent electron transport ability in the presence of the rGO platform. As the Ag@Cu₂O interacted with rGO, the available surplus electrons increased, which increased the chances for 4-NP to randomly adsorb on the surface of the Ag@Cu₂O-rGO. More importantly, the proposed Ag@Cu₂O-rGO nanomaterials have a high absorption, and they are expected to have significantly enhanced catalytic activity for 4-NP. The designed Ag@Cu₂O-rGO composites have potential application in a catalytic system for removing toxic and harmful substances in water. This graphene-based catalytic study is important for the application and development of nanomaterial science.

Author Contributions: Methodology, formal analysis, writing—original draft preparation, C.S.; validation and formal analysis, S.G.; data curation, writing—review and editing and funding acquisition, L.C.; All authors have read and agreed to the published version of the manuscript.

Funding: This research was funded by the project of Jilin Development and Reform Commission (No. 2019C051-3).

Institutional Review Board Statement: Not applicable for studies over humans or animals.

Informed Consent Statement: Not applicable for studies over humans.

Data Availability Statement: Data available in a publicly accessible repository.

Conflicts of Interest: The authors declare no conflict of interest.

References

1. Yury, G. Transition metal carbides go 2D nature nanotechnology. *Nat. Mater.* **2015**, *14*, 1079–1080.
2. Tian, H.W.; Liu, M.; Zheng, W.T. Constructing 2D graphitic carbon nitride nanosheets/layered MoS₂/graphene ternary nanojunction with enhanced photocatalytic activity. *Appl. Catal. B Environ.* **2018**, *225*, 468–476. [[CrossRef](#)]
3. Lee, Y.T.; Jeon, P.J.; Han, J.H.; Ahn, J.; Lee, H.S.; Lim, J.Y.; Choi, W.K.; Song, J.D.; Park, M.; Lm, S.; et al. Mixed-dimensional 1D ZnO-2D WSe₂ van derWaals heterojunction device for photosensor. *Adv. Funct. Mater.* **2018**, *27*, 1703822–1703830. [[CrossRef](#)]
4. Jariwala, D.; Sangwan, V.K.; Lauhon, L.J.; Marks, T.J.; Hersam, M.C. Emerging device applications for semiconducting two-dimensional transition metal dichalcogenides. *ACS Nano* **2014**, *8*, 1102–1122. [[CrossRef](#)] [[PubMed](#)]
5. Tan, C.; Cao, X.; Wu, X.J.; He, Q.; Yang, J.; Zhang, X.; Chen, J.; Zhao, W.; Han, S.; Nam, G.-H.; et al. Recent advances in ultrathin two-dimensional nanomaterials. *Chem. Rev.* **2017**, *117*, 6225–6331. [[CrossRef](#)] [[PubMed](#)]
6. Yang, M.-Q.; Dan, J.; Pennycook, S.J.; Lu, X.; Zhu, H.; Xu, Q.-H.; Fan, H.J.; Ho, G.W. Ultrathin nickel boron oxide nanosheets assembled vertically on graphene: A new hybrid 2D material for enhanced photo/electro-catalysis. *Mater. Horiz.* **2017**, *4*, 885–894. [[CrossRef](#)]
7. Han, C.; Lu, Y.; Zhang, J.; Ge, L.; Li, Y.; Chen, C.; Xin, Y.; Wu, L.; Fang, S. Novel PtCo alloy nanoparticle decorated 2D g-C₃N₄ nanosheets with enhanced photocatalytic activity for H₂ evolution under visible light irradiation. *J. Mater. Chem. A* **2015**, *3*, 23274–23282. [[CrossRef](#)]
8. Fu, X.-L.; Fang, H.; Liu, F.-R.; Ren, S.-W.; Cao, J.-T.; Liu, Y.-M. Electrochemiluminescence energy resonance transfer in 2D/2D heterostructured g-C₃N₄/MnO₂ for glutathione detection. *Biosens. Bioelectron.* **2019**, *129*, 72–78. [[CrossRef](#)]
9. Kumar, R.; Goel, N.; Kumar, M. UV-activated MoS₂ based fast and reversible NO₂ sensor at room temperature. *ACS Sens.* **2017**, *2*, 1744–1752. [[CrossRef](#)]
10. Tu, Z.; Guy, G.; Mohsen, A.; Haag, R. Multivalent interactions between 2D nanomaterials and biointerfaces. *Adv. Mater.* **2018**, *30*, 1706709–1706735. [[CrossRef](#)]
11. Zhang, Z.; Huang, J.; Zhang, M.; Yuan, Q.; Dong, B. Ultrathin hexagonal SnS₂ nanosheets coupled with g-C₃N₄ nanosheets as 2D/2D heterojunction photocatalysts toward high photocatalytic activity. *Appl. Catal. B Environ.* **2015**, *163*, 298–305. [[CrossRef](#)]

12. Singh, A.; Khare, P.; Verma, S.; Bhati, A.; Sonker, A.K.; Tripathi, K.M.; Sonkar, S.K. Pollutant soot for pollutant dye degradation: Soluble graphene nanosheets for visible light induced photodegradation of methylene blue. *ACS Sustain. Chem. Eng.* **2017**, *5*, 8860–8869. [[CrossRef](#)]
13. Miller, O.D.; Ilic, O.; Christensen, T.; Reid, M.T.H.; Atwater, H.A.; Joannopoulos, J.D.; Soljačić, M.; Johnson, S.G. Limits to the optical response of graphene and two-dimensional materials. *Nano Lett.* **2017**, *17*, 5408–5415. [[CrossRef](#)] [[PubMed](#)]
14. Novoselov, K.S.; Geim, A.K.; Morozov, S.V. Electric field effect in atomically thin carbon films. *Science* **2004**, *306*, 666–669. [[CrossRef](#)] [[PubMed](#)]
15. Atkin, P.; Daenke, T.; Wang, Y.; Carey, B.J.; Berean, K.J.; Clark, R.M.; Ou, J.Z.; Trinchì, A.; Cole, I.S.; Kalantar-Zadeh, K. 2D WS₂/carbon dot hybrids with enhanced photocatalytic activity. *J. Mater. Chem. A* **2016**, *4*, 13563–13571. [[CrossRef](#)]
16. Li, Z.-X.; Yang, B.-L.; Zou, K.-Y.; Kong, L.; Yue, M.-L.; Duan, H.-H. Novel porous carbon nanosheet derived from a 2D Cu-MOF: Ultrahigh porosity and excellent performances in the supercapacitor cell. *Carbon* **2019**, *144*, 540–548. [[CrossRef](#)]
17. Jeon, Y.J.; Yun, J.M.; Kang, M.; Lee, S.; Jung, Y.-S.; Hwang, K.; Heo, Y.-J.; Kim, J.-E.; Kang, R.; Kim, D.-Y. 2D/2D vanadyl phosphate (VP) on reduced graphene oxide as a hole transporting layer for efficient organic solar cells. *Org. Electron.* **2018**, *59*, 92–98. [[CrossRef](#)]
18. Marcano, D.C.; Kosynkin, D.V.; Berlin, J.M.; Sinitskii, A.; Sun, Z.; Slesarev, A.; Alemany, L.B.; Lu, W.; Tour, J.M. Improved synthesis of graphene oxide. *ACS Nano* **2010**, *4*, 4806–4814. [[CrossRef](#)]
19. Xu, W.; Mao, N.; Zhang, J. Graphene: A platform for surface-enhanced raman spectroscopy. *Small* **2013**, *9*, 1206–1224. [[CrossRef](#)]
20. Zhu, A.; Qiao, L.; Jia, Z.; Tan, P.; Liu, Y.; Ma, Y.; Pan, J. C-S bonds induced ultrafine SnS₂ dots/porous g-C₃N₄ sheets 0D/2D heterojunction: Synthesis and photocatalytic mechanism investigation. *Dalton Trans.* **2017**, *46*, 17032–17040. [[CrossRef](#)]
21. Guo, J.; Jiang, D. Covalent organic frameworks for heterogeneous catalysis: Principle, current status, and challenges. *ACS Cent. Sci.* **2020**, *6*, 869–879. [[CrossRef](#)] [[PubMed](#)]
22. Wu, Q.; Liang, M.; Zhang, S.; Liu, X.; Wang, F. Development of functional black phosphorus nanosheets with remarkable catalytic and antibacterial performance. *Nanoscale* **2018**, *10*, 10428–10435. [[CrossRef](#)] [[PubMed](#)]
23. Fu, Q.; Draxl, C. Hybrid organic-inorganic perovskites as promising substrates for Pt single-atom catalysts. *Phys. Rev. Lett.* **2019**, *122*, 046101. [[CrossRef](#)] [[PubMed](#)]
24. Chen, L.; Liu, M.M.; Zhao, Y.; Kou, Q.; Wang, Y.; Liu, Y.; Zhang, Y.; Yang, J.; Jung, Y.M. Enhanced catalyst activity by decorating of Au on Ag@Cu₂O nanoshell. *Appl. Surf. Sci.* **2018**, *435*, 72–78. [[CrossRef](#)]
25. Li, Y.; Cain, J.D.; Hanson, E.D.; Murthy, A.A.; Hao, S.; Shi, F.; Li, Q.; Wolverson, C.; Chen, X.; Dravid, V.P. Au@MoS₂ core-shell heterostructures with strong light-matter interactions. *Nano Lett.* **2016**, *16*, 7696–7702. [[CrossRef](#)] [[PubMed](#)]
26. Zhang, X.Y.; Han, D.L.; Pang, Z.Y.; Sun, Y.; Wang, Y.; Zhang, Y.; Yang, J.; Chen, L. Charge transfer in an ordered Ag/Cu₂S/4-MBA system based on surface-enhanced Raman scattering. *J. Phys. Chem. C* **2018**, *122*, 5599–5605. [[CrossRef](#)]
27. Zhu, W.; Crozier, K.B. Quantum mechanical limit to plasmonic enhancement as observed by surface-enhanced Raman scattering. *Nat. Commun.* **2014**, *5*, 5228–5235. [[CrossRef](#)]
28. Xu, L.; Zhang, F.; Song, X.; Yin, Z.; Bu, Y. Construction of reduced graphene oxide-supported Ag-Cu₂O composites with hierarchical structures for enhanced photocatalytic activities and recyclability. *J. Mater. Chem. A* **2015**, *3*, 5923–5933. [[CrossRef](#)]
29. Guo, Y.; Wang, H.; Ma, X.; Jin, J.; Ji, W.; Wang, X.; Song, W.; Zhao, B.; He, C. Fabrication of Ag-Cu₂O/reduced graphene oxide nanocomposites as SERS substrates for in situ monitoring of peroxidase-like catalytic reaction and biosensing. *ACS Appl. Mater. Int.* **2017**, *9*, 19074–19081. [[CrossRef](#)]
30. Mahmoud, M.A.; Qian, W.; El-Sayed, M.A. Following charge separation on the nanoscale in Cu₂O-Au nanoframe hollow nanoparticles. *Nano Lett.* **2011**, *11*, 3285–3289. [[CrossRef](#)]
31. Huang, J.; Vongehr, S.; Tang, S.; Lu, H.; Shen, J.; Meng, X. Ag dendrite-based Au/Ag bimetallic nanostructures with strongly enhanced catalytic activity. *Langmuir* **2009**, *25*, 11890–11896. [[CrossRef](#)] [[PubMed](#)]
32. Lee, P.C.; Meisel, D. Adsorption and surface-enhanced Raman of dyes on silver and gold sols. *J. Phys. Chem.* **1982**, *86*, 3391–3395. [[CrossRef](#)]
33. Hummers, W.S.; Offeman, R.E. Preparation of graphitic oxide. *J. Am. Chem. Soc.* **1958**, *80*, 1339. [[CrossRef](#)]